Title

Thermal Fault Diagnostics in Lithium-ion Batteries based on a Distributed Parameter Thermal Model

Authors

Dey, Satadru, PhD
Perez, Hector E, PhD
Moura, Scott J, PhD

Publication Date

2016-10-30

Thermal Fault Diagnostics in Lithium-ion Batteries based on a Distributed Parameter Thermal Model

Satadru Dey, Hector E. Perez and Scott J. Moura

Abstract— **Lithium-ion (Li-ion) battery faults or failure mechanisms are potentially hazardous to battery health, safety and performance. Thermal fault mechanisms represent a critical subset of such failures. To ensure safety and reliability, battery management systems must have the capability of diagnosing these thermal failures. In line with this requirement, we present a Partial Differential Equation (PDE) model-based scheme for diagnosing thermal faults in Li-ion batteries. For this study, we adopt a distributed parameter one-dimensional thermal model for cylindrical battery cells. The diagnostic scheme objective is to detect and estimate the size of the thermal fault. The scheme consists of two PDE observers arranged in cascade with measured surface temperature feedback. The first observer, denoted as *Robust Observer*, estimates the distributed temperature inside the cell under nominal (healthy) and faulty conditions. The second observer, denoted as *Diagnostic Observer*, receives this estimated temperature distribution, and in turn outputs a residual signal that provides the fault information. Furthermore, the residual signal is evaluated against non-zero thresholds to achieve robustness against modeling and measurement uncertainties. Lyapunov stability theory has been utilized to verify the analytical convergence of the observers under heathy and faulty conditions. Simulation studies are presented to illustrate the effectiveness of the proposed scheme.**

I. INTRODUCTION

Lithium-ion (Li-ion) batteries are the key energy storage devices in automotive, power grid and portable electronics applications. Performance, safety and reliability are crucial aspects of Li-ion battery operation. Several failure mechanisms, ranging from internal micro-scale failures to external sensor faults, can potentially deteriorate battery performance and safety. Thermal failure and degradation mechanisms constitute an important subset of such factors [1]. Some of these thermal failures, e.g. thermal runaway, may even lead to catastrophic events if not detected or diagnosed early enough. Therefore, diagnosis of battery thermal failures is extremely important to ensure safe and reliable operation. In this paper, we propose a Partial Differential Equation (PDE) model-based diagnosis scheme for thermal faults in Li-ion batteries.

In the battery controls/estimation literature, real-time estimation of State-of-Charge (SOC) and State-of-Health (SOH) have received substantial attention in the past decade. Broadly, these estimation approaches can be divided into two major categories based on the type of model used: (i) Equivalent Circuit Model based approaches [2] [3] [4] [5] [6] and, (ii) Electrochemical Model based approaches [7] [8] [9] [10]. Compared to SOC and SOH estimation, temperature estimation problems have received significantly less attention. There are some recent studies. For example, an adaptive observer is presented for core temperature estimation in [11]. Observer design for temperature estimation in battery packs is studied in [12]. In [13], an internal temperature estimation algorithm is proposed using combined impedance and surface temperature measurements. In [14], an algorithm is presented for estimation of the temperature distribution in cylindrical cells under unknown cooling conditions.

The body of literature on real-time fault diagnosis problems in batteries is significantly smaller than estimation problems. Some of the existing approaches deal with sensor and actuator faults [15] [16] [17], electrochemical faults [18], overcharge/over-discharge faults [19], and terminal voltage collapse [20]. However, real-time diagnosis of thermal faults is almost unexplored in the existing published literature, despite its critical importance for battery safety and performance. A few efforts exist in battery thermal fault diagnostics. In [15], a one state thermal model capturing the averaged temperature of the battery cell is used to diagnose a cooling system fault. A two-state thermal model capturing the core and surface temperature dynamics is used in [21] to diagnose certain thermal faults. These approaches, however, (i) rely on lumped parameter thermal models which may not be sufficient to capture the effect of distributed thermal faults inside the cell, and (ii) do not estimate fault size. Note that information on fault size can be crucial for thermal management under faulty conditions. In the present paper, we extend this research by proposing a battery thermal fault diagnosis scheme which (i) utilizes a distributed parameter thermal model and, (ii) detects and estimates the thermal fault size.

In the proposed diagnostic scheme, we adopt a one-dimensional distributed parameter thermal model of a cylindrical battery cell [22]. The scheme consists of two PDE observers arranged in cascade and utilizes measured surface temperature feedback. The first observer, denoted as *Robust Observer*, estimates the distributed temperature inside the cell under healthy and faulty conditions. Robust state estimation is a bi-product of this scheme that provides convergent estimates of the temperature distribution inside the battery cell irrespective of healthy or faulty conditions. The second observer, denoted as *Diagnostic Observer*, receives this estimated temperature distribution information from *Robust Observer* and in turn outputs a residual signal that provides the fault information. The backstepping transformation and Lyapunov stability [23] have been utilized to design and

S. Dey, H. E. Perez and S. J. Moura are with Department of Civil and Environmental Engineering, University of California, Berkeley, CA 94720, USA satadru86@berkeley.edu, heperez@berkeley.edu, smoura@berkeley.edu.

analyze the observer. Furthermore, the residual signals are compared with non-zero thresholds to incorporate robustness to modeling and measurement uncertainties. These non-zero thresholds are designed offline based on the probability distribution of the residual signals under a fault-free condition.

The rest of the paper is organized as follows. Section II introduces the distributed parameter thermal model of the battery cell. Section III designs and analyzes the fault diagnosis scheme in detail. Simulation studies are presented in Section IV. Finally, Section V concludes the work.

Notations: In this paper, following notations are used: $\|u(\cdot)\| = \sqrt{\int_0^1 u^2(x)dx}$, $u_t = \frac{\partial u}{\partial t}, u_x = \frac{\partial u}{\partial x}$, $u_{xx} = \frac{\partial^2 u}{\partial x^2}$.

II. DISTRIBUTED PARAMETER THERMAL MODEL FOR LI-ION BATTERIES

Nominal Model: We adopt the following (nominal or fault-free) one-dimensional thermal model that predicts the radially distributed temperature dynamics of a cylindrical battery cell (Fig. 1) [22]:

$$\beta \frac{\partial \bar{T}}{\partial \bar{t}}(r,\bar{t}) = \frac{\partial^2 \bar{T}}{\partial r^2}(r,\bar{t}) + \left(\frac{1}{r}\right)\frac{\partial \bar{T}}{\partial r}(r,\bar{t}) + \frac{\dot{Q}(\bar{t})}{\bar{k}} \tag{1}$$

with Neumann boundary conditions

$$\frac{\partial \bar{T}}{\partial r}(0,\bar{t}) = 0, \tag{2}$$

$$\frac{\partial \bar{T}}{\partial r}(R,\bar{t}) = \frac{h}{\bar{k}}\left(T_\infty - \bar{T}\left(R,\bar{t}\right)\right), \tag{3}$$

where $\bar{t} \in \mathbb{R}^+$ represents time and $r \in [0,R]$ is the spatial coordinate in the radial direction. The parameter $\bar{k}$ is the thermal conductivity of the battery cell, $\dot{Q}(\bar{t})$ is the volumetric heat generation rate, and $\beta = (\rho C_p)/\bar{k}$ is the inverse of thermal diffusivity, where ρ is the mass density and C_p is the specific heat capacity.

Next, we: i) transform the system to the Cartesian coordinate system with spatial coordinate variable $\bar{x}$ and time $\bar{t}$ and, ii) scale the space and time variables in the Cartesian coordinate system by defining $T\left(x,t\right) = \bar{T}\left(\bar{x},\bar{t}\right)$ with $x = \bar{x}/R$, $t = \bar{t}/\beta R^2$ and $k = \bar{k}/R^2$. This transformation and scaling results in the following system, known as a heat equation:

$$T_t(x,t) = T_{xx}(x,t) + \frac{\dot{Q}(t)}{k}, \tag{4}$$

with Neumann boundary conditions

$$T_x(0,t) = 0, \tag{5}$$

$$T_x(1,t) = \frac{h}{k}\left(T_\infty - T\left(1,t\right)\right), \tag{6}$$

where $t \in \mathbb{R}^+$ and $x \in [0,1]$. The remainder of this paper considers (4)-(6) as the plant model.

Furthermore, we adopt a second order electric circuit model to capture the electrical dynamics of the battery (see Fig. 2) [24]. The electrical circuit consists of an open circuit voltage source (V_{oc}), an internal series resistance (R_{int}) and two resistance-capacitance branches in series. Furthermore, it is assumed that the SOC of the battery is computed online via Coulomb-counting. The state-space equations for the electrical model are:

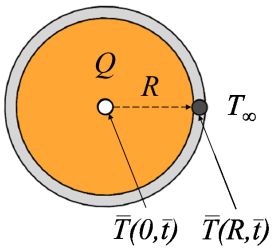

Fig. 1. Schematic of the electro-thermal battery model

$$\frac{dSOC}{dt}(t) = -\frac{I(t)}{C_{batt}}, \tag{7}$$

$$\frac{dV_1}{dt}(t) = -\frac{V_1(t)}{R_1C_1} + \frac{I(t)}{C_1}, \tag{8}$$

$$\frac{dV_2}{dt}(t) = -\frac{V_2(t)}{R_2C_2} + \frac{I(t)}{C_2}, \tag{9}$$

$$V_{term}(t) = V_{oc}(SOC) - V_1(t) - V_2(t) - R_{int}I(t), \tag{10}$$

where $I(t)$ is the battery current, C_{batt} is the battery charge capacity in Ah and V_{term} is the terminal voltage. The open circuit voltage (V_{oc}) is a function of the State-of-Charge (SOC) and computed online. This function can be determined via offline experimental studies. In this distributed parameter model, R_{int} is assumed to have Arrhenius dependence on the average battery temperature T_{avg} given as:

$$R_{int} = f\left(T_{avg}\right), \tag{11}$$

where $f\left(T_{avg}\right) = R_{int,ref} \cdot \exp\left(\frac{T_{ref}}{T_{avg}}\right)$ and $R_{int,ref}$ is a known reference value at a known reference temperature T_{ref}. Figure 3 provides a schematic of the coupled electrical-thermal model. The average temperature of the cell is given by:

$$T_{avg}(t) = \int_0^1 T\left(x,t\right)dx. \tag{12}$$

Measurements: Measured variables include the current (I), terminal voltage (V_{term}), and surface temperature $(T(1))$.

Remark 1. The heat generation rate Q is expressed as:

$$\dot{Q}(t) = I(t)(V_{oc}(SOC) - V_{term}(t)). \tag{13}$$

In this work we assume that $\dot{Q}$ is computed online using the measured variables V_{term}, I, and $V_{oc}(SOC)$, which is computed using the SOC information from (7). Furthermore, we assume that the electrical states V_1 and V_2 are computed online via the open-loop model (8)-(9).

Fault Model: The faulty battery thermal dynamics can be mathematically modeled as

$$T_t(x,t) = T_{xx}(x,t) + \frac{Q(t)}{k} + \Delta_Q(x,t), \tag{14}$$

with Neumann boundary conditions

$$T_x(0,t) = 0, \tag{15}$$

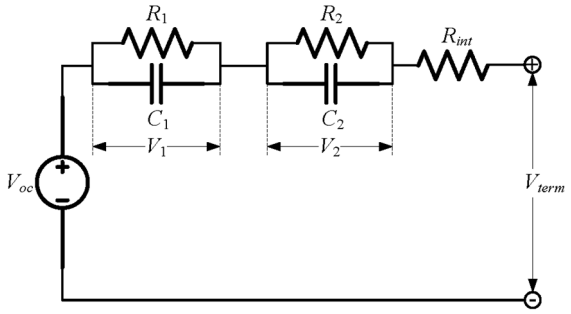

Fig. 2. Battery electrical circuit model

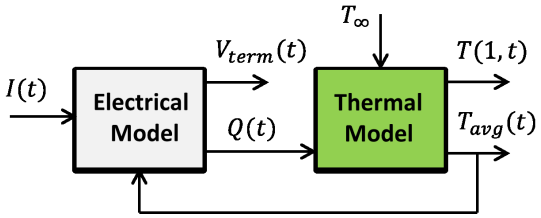

Fig. 3. Schematic of the electro-thermal battery model

$$T_x(1,t) = \frac{h}{k}\left(T_\infty - T\left(1\right)\right), \tag{16}$$

where $\Delta_Q(x,t)$ represents a distributed thermal fault, such as abnormal internal heat generation from electrochemical side reactions, or internal failure due to mechanical or thermal abuse [1][25].

III. FAULT DIAGNOSIS SCHEME

The fault diagnosis scheme is diagramed in Fig. 4. The scheme consists of two observers working in a cascaded manner. The first observer, *Robust Observer*, uses the surface temperature feedback and estimates the distributed battery cell temperature under healthy (non-faulty) and faulty condition. The second observer, *Diagnostic Observer*, receives the estimated temperature distribution from *Robust Observer* and in turn provides a residual signal. The residual signal is used for detection and estimation of the thermal fault (Δ_Q). In the next subsections, we will discuss the design of these two observers in detail.

Remark 2. The proposed diagnostic scheme provides an accurate estimation of the temperature distribution inside the battery cell irrespective of faulty or healthy condition. This is an additional beneficial feature of this scheme.

A. Robust Observer

The following structure is chosen for the *Robust Observer*,

$$\hat{T}_{1t}(x,t) = \hat{T}_{1xx}(x,t) + \frac{Q(t)}{k} + P_1(x)\tilde{T}_1(1,t), \tag{17}$$

with Neumann boundary conditions

$$\hat{T}_{1x}(0,t) = 0, \tag{18}$$

$$\hat{T}_{1x}(1,t) = \frac{h}{k}\left(T_\infty - T\left(1,t\right)\right) + P_{10}\tilde{T}_1(1,t), \tag{19}$$

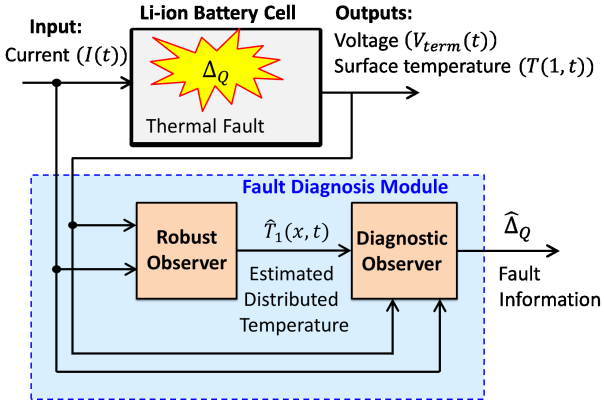

Fig. 4. Fault diagnosis scheme

where $\hat{T}_1(x,t)$ is the estimated temperature distribution, $\tilde{T}_1(1,t) = T(1,t) - \hat{T}_1(1,t)$ is the boundary estimation error and $P_1(x)$ and P_{10} are the observer gains to be determined.

The error dynamics of the *Robust Observer* are given by subtracting (17)-(19) from (14)-(16),

$$\tilde{T}_{1t}(x,t) = \tilde{T}_{1xx}(x,t) + \Delta_Q(x,t) - P_1(x)\tilde{T}_1(1,t), \tag{20}$$

$$\tilde{T}_{1x}(0,t) = 0, \tag{21}$$

$$\tilde{T}_{1x}(1,t) = -P_{10}\tilde{T}_1(1,t). \tag{22}$$

Next, we follow the backstepping approach to analyze the error dynamics and design the observer gains [23]. The backstepping approach seeks the linear Volterra transformation $\tilde{T}_1(x,t) \mapsto \omega(x,t)$

$$\tilde{T}_1(x,t) = \omega(x,t) - \int_x^1 P(x,y)\omega(y,t)dy, \tag{23}$$

which transforms (20)-(22) to the following target error system

$$\omega_t(x,t) = \omega_{xx}(x,t) + \Delta_{\omega Q}(x,t) - c\omega(x,t), \tag{24}$$

$$\omega_x(0,t) = 0, \tag{25}$$

$$\omega_x(1,t) = 0, \tag{26}$$

with $c > 0$ as a parameter of user's choice and $\Delta_Q(x,t) = \Delta_{\omega Q}(x,t) - \int_x^1 P(x,y)\Delta_{\omega Q}(y,t)dy$. Note that, the gain kernel $P(x,y)$ in (23) must satisfy the following conditions:

$$P_{yy}(x,y) - P_{xx}(x,y) = cP(x,y), \tag{27}$$

$$P(x,x) = -c\frac{x}{2}, \tag{28}$$

$$P_x(0,y) = 0, \tag{29}$$

and the observer gains can be computed as:

$$P_1(x) = -P_y(x,1), \tag{30}$$

$$P_{10} = -P(1,1), \tag{31}$$

Remark 3. There exists a unique and closed-form solution of the kernel PDE (27)-(29) [23], given by

$$P(x,y) = -cy\frac{I_1(\sqrt{c(y^2-x^2)})}{\sqrt{c(y^2-x^2)}}. \tag{32}$$

Therefore, the observer gains can be computed offline via (30)-(31) using the closed form solution (32).

Remark 4. It can be proven that the transformation (23) is invertible [23]. Hence, stability of the target system (24)-(26) implies stability of the original system (20)-(22). Next, we present a theorem for the convergence of the *Robust Observer* via stability analysis of the target system.

Theorem 1 (Convergence of Robust Observer)**.** *Consider the error dynamics (24)-(26). If $c > 0$, then*
(a) under Scenario 1: $\Delta_{\omega Q} = 0$ i.e. in presence of no fault, the origin of the error space $\omega(x,t) = 0$ is exponentially stable in the sense of spatial $\mathcal{H}_1$ norm. Furthermore, it can also be shown that $\omega(x,t) \to 0, \forall x \in [0,1]$ as $t \to \infty$.
(b) under Scenario 2: $\Delta_{\omega Q} \neq 0$ i.e. in presence of the fault, the error $\omega(x,t)$ converges to a ball of radius (in the sense of spatial $\mathcal{H}_1$ norm) defined by $R_B = \frac{\|\Delta_{\omega Q}\|^2 + \|\Delta_{\omega Qx}\|^2}{2c^2}$. Note that the magnitude of R_B can be made arbitrarily small by choice of a high value of c. Furthermore, it can also be shown that $\omega(x,t), \forall x \in [0,1]$ settles to a bounded region as $t \to \infty$.

Proof. We consider the spatial $\mathcal{H}_1$ norm as a Lyapunov function candidate to analyze the error dynamics (24)-(26):

$$W_1(t) = \frac{\|\omega\|^2 + \|\omega_x\|^2}{2} \tag{33}$$

$$\triangleq \frac{1}{2}\int_0^1 \omega^2(x,t)dx + \frac{1}{2}\int_0^1 \omega_x^2(x,t)dx. \tag{34}$$

The derivative of $W_1(t)$ along the state trajectory can be written as:

$$\dot{W}_1(t) = \int_0^1 \omega\omega_t dx + \int_0^1 \omega_x\omega_{xt}dx. \tag{35}$$

Now consider the first term of the right hand side of (35),

$$\int_0^1 \omega\omega_t dx = \int_0^1 \omega\omega_{xx}dx + \int_0^1 \omega\Delta_{\omega Q}dx - c\int_0^1 \omega^2 dx. \tag{36}$$

Applying Cauchy-Schwarz inequality on the second term and integration by parts on the first term of the right hand side of (36) yields

$$\int_0^1 \omega\omega_t dx \leq -\|\omega_x\|^2 + \|\omega\|\,\|\Delta_{\omega Q}\| - c\|\omega\|^2 \tag{37}$$

Now applying integration by parts on the second term of right hand side of (35), we have

$$\int_0^1 \omega_x\omega_{xt}dx = -\int_0^1 \omega_t\omega_{xx}dx$$

$$= -\int_0^1 \omega_{xx}^2 dx - \int_0^1 \omega_{xx}\Delta_{\omega Q} + c\int_0^1 \omega\omega_{xx}dx. \tag{38}$$

Next applying integration by parts on the second and third terms of the right hand side of (38), we have

$$\int_0^1 \omega_x\omega_{xt}dx = -\int_0^1 \omega_{xx}^2 dx + \int_0^1 \omega_x\Delta_{\omega Qx} - c\int_0^1 \omega_x^2 dx \tag{39}$$

Further, we apply Cauchy-Schwarz inequality on the second term of right hand side of (39) which yields

$$\int_0^1 \omega_x\omega_{xt}dx \leq -\|\omega_{xx}\|^2 + \|\Delta_{\omega Qx}\|\,\|\omega_x\| - c\|\omega_x\|^2. \tag{40}$$

Finally, considering (37) and (40) we can write the upper bound of the derivative of the Lyapunov function

$$\dot{W}_1(t) \leq \|\omega\|(\|\Delta_{\omega Q}\| - c\|\omega\|) + \|\omega_x\|(\|\Delta_{\omega Qx}\| - c\|\omega_x\|). \tag{41}$$

Now considering *Scenario 1:* $\Delta_{\omega Q} = 0$, we can write (41) as

$$\dot{W}_1(t) \leq -2cW_1(t). \tag{42}$$

If $c > 0$ the solution of the differential inequality (42) is $W_1(t) \leq W_1(0)\exp(-2ct)$ which confirms the exponential convergence of $W_1(t)$. Next, using Agmon's inequality we can write that

$$\max_{x\in[0,1]} |\omega(x,t)|^2 \leq 2\|\omega\|\,\|\omega_x\| \leq \|\omega\|^2 + \|\omega_x\|^2 = 2W_1(t). \tag{43}$$

Therefore, from the knowledge of $W_1(t) \to 0$ as $t \to \infty$ and (43), we prove that $\omega(x,t) \to 0, \forall x \in [0,1]$ as $t \to \infty$. Next, we consider *Scenario 2:* $\Delta_{\omega Q} \neq 0$. From (41), the sufficient conditions for the negative definiteness of $\dot{W}_1(t)$ are

$$\|\omega\| > \frac{\|\Delta_{\omega Q}\|}{c}, \|\omega_x\| > \frac{\|\Delta_{\omega Qx}\|}{c}. \tag{44}$$

Squaring both sides of the conditions in (44) and adding them, we can write a single sufficiency condition as

$$\frac{\|\omega\|^2 + \|\omega_x\|^2}{2} > R_B \triangleq \frac{\|\Delta_{\omega Q}\|^2 + \|\Delta_{\omega Qx}\|^2}{2c^2}. \tag{45}$$

Therefore, we can conclude that the negative definiteness of $\dot{W}_1(t)$ will hold outside the ball of radius in the $\|\omega\|_{\mathcal{H}_1}$ space defined by R_B. Hence, $W_1(t)$ will settle on or within a bounded ball of radius R_B. Note that the magnitude of R_B can be made arbitrarily small by choosing a high value of c. Next, considering the boundedness of $W_1(t)$ and following the same argument as in (43), we can conclude that $\omega(x,t), \forall x \in [0,1]$ settles to a bounded region as $t \to \infty$. □

B. Diagnostic Observer

The *Diagnostic Observer* utilizes the estimated temperature distribution from *Robust Observer* as a feedback signal.

Remark 5. The estimated temperature distribution from *Robust Observer* can be written as:

$$\hat{T}_1(x,t) = T(x,t) + \epsilon(x,t).$$

However, we have proven that ϵ can be made arbitrarily small by selecting c arbitrarily large. Therefore, we consider $\hat{T}_1(x,t) \approx T(x,t)$ for all practical purposes in the following analysis.

Assumption 1. We assume the following structure of the fault function

$$\Delta_Q(x,t) = \theta\psi(T(x,t), I(t)) \tag{46}$$

where $\psi(\cdot,\cdot)$ is a known function of distributed state $T(x,t)$ and input current I, and $\theta \in \mathbb{R}$ is an unknown constant parameter which determines the fault size. The main objective of the diagnostic observer is to estimate the value of θ.

Considering *Remark 5* and *Assumption 1*, the following structure is chosen for the *Diagnostic Observer*,

$$\hat{T}_{2t}(x,t) = \hat{T}_{2xx}(x,t) + \frac{Q(t)}{k} + \hat{\theta}\psi(T(x,t),I(t)) + L_2\tilde{T}_2(x,t), \tag{47}$$

with Neumann boundary conditions

$$\hat{T}_{2x}(0,t) = 0, \tag{48}$$

$$\hat{T}_{2x}(1,t) = \frac{h}{k}\left(T_\infty - T\left(1,t\right)\right), \tag{49}$$

where $\hat{T}_2(x,t)$ is the estimated temperature distribution by *Diagnostic Observer*, $\tilde{T}_2(x,t) = T(x,t) - \hat{T}_2(x,t)$ is the distributed estimation error with $T(x,t)$ as the estimated temperature distribution from *Robust Observer*, $\hat{\theta}$ is the estimated size of the fault and, $L_2 \in \mathbb{R}$ is an observer gain to be determined. The update law for $\hat{\theta}$ is chosen as

$$\dot{\hat{\theta}} = \frac{1}{L_3}\int_0^1 \psi(T(x,t),I(t))\tilde{T}_2(x,t)dx, \tag{50}$$

where $L_3 > 0$ is a user-defined gain that determines the parameter convergence rate. Subtracting (47)-(49) from (14)-(16), we can write the error dynamics of *Diagnostic Observer* as

$$\tilde{T}_{2t}(x,t) = \tilde{T}_{2xx}(x,t) + \tilde{\theta}\psi(T(x,t),I(t)) - L_2\tilde{T}_2(x,t), \tag{51}$$

with Neumann boundary conditions

$$\tilde{T}_{2x}(0,t) = \tilde{T}_{2x}(1,t) = 0, \tag{52}$$

In the following theorem, we analyze the performance of the *Diagnostic Observer*.

Theorem 2 (Performance of Diagnostic Observer)**.** *Consider the error dynamics (51)-(52) and the parameter update law (50). If Remark 5 and Assumption 1 are valid and $L_2 \geq -\frac{1}{4}$, then the distributed state estimation error $\tilde{T}_2(x,t)$ and parameter estimation error $\tilde{\theta}$ will be bounded. i.e. $\left\|\tilde{T}_2\right\|, \left|\tilde{\theta}\right| \in \mathbb{L}_\infty$ as $t \to \infty$.*

Proof. We consider the following Lyapunov function candidate to analyze the error dynamics

$$W_2(t) = \frac{1}{2}\int_0^1 \tilde{T}_2^2(x,t)dx + \frac{L_3}{2}\tilde{\theta}^2 \tag{53}$$

The derivative of $W_2(t)$ along the state trajectories can be written as:

$$\dot{W}_2(t) = \int_0^1 \tilde{T}_2\tilde{T}_{2t}dx + L_3\tilde{\theta}\dot{\tilde{\theta}} \tag{54}$$

Now considering (51) and the fact $\dot{\theta} = 0$, we can write

$$\begin{aligned}\dot{W}_2(t) = \int_0^1 \tilde{T}_2\tilde{T}_{2xx}dx - L_2\int_0^1 \tilde{T}_2^2dx \\ +\tilde{\theta}\int_0^1 \psi(T,I)\tilde{T}_2dx - L_3\tilde{\theta}\dot{\tilde{\theta}}\end{aligned} \tag{55}$$

Next applying integration by parts on the first term of the right hand side of (55) and then applying Poincaré inequality: $-\int_0^1 \tilde{T}_{2x}^2dx \leq -\frac{1}{4}\int_0^1 \tilde{T}_2^2dx$, we have

$$\begin{aligned}\dot{W}_2(t) \leq -\frac{1}{4}\int_0^1 \tilde{T}_2^2dx - L_2\int_0^1 \tilde{T}_2^2dx \\ +\tilde{\theta}\int_0^1 \psi(T,I)\tilde{T}_2dx - L_3\tilde{\theta}\dot{\tilde{\theta}}\end{aligned} \tag{56}$$

Finally, applying the update law (50) on (56), we can write:

$$\dot{W}_2(t) \leq -(\frac{1}{4} + L_2)\int_0^1 \tilde{T}_2^2dx. \tag{57}$$

From (57) it can be concluded that $\dot{W}_2(t)$ is negative semidefinite if $L_2 \geq -\frac{1}{4}$. Hence, the estimation errors $\left|\tilde{\theta}\right|$ and $\tilde{T}_2(x,t)$ will be bounded. i.e. $\left\|\tilde{T}_2\right\|, \left|\tilde{\theta}\right| \in \mathbb{L}_\infty$ as $t \to \infty$. □

Remark 6. The parameter estimate $\hat{\theta}$ will be used as a residual signal which serves the purpose of detection (indicated by the fact $\hat{\theta} \neq 0$) and estimation (indicated by the magnitude of $\hat{\theta}$) of the thermal fault Δ_Q.

C. Robustness to Uncertainties

Uncertainties, such as unmodeled dynamics and measurement noise, have not been considered in the diagnostic scheme design. The presence of these uncertainties prohibits the residual $\hat{\theta}$ from having the idealized property of equaling zero in the absence of a fault. One approach to handle this issue is to use nonzero thresholds. The residuals will be evaluated as follows: Fault is detected when $\hat{\theta} > th$; no fault when $\hat{\theta} \leq th$, where th is the predefined threshold. The effect of the uncertainties on the residuals will be suppressed below these threshold values.

Below are the guidelines for selection of constant threshold values for the evaluation of the residual:
Step 1: Collect residual data under non-faulty conditions from Monte-Carlo simulations or experimental studies.
Step 2: Plot the probability distribution of the residual data. In general, this probability distribution will depend on the statistics of the uncertainties and dynamic system structure in the experimental data or Monte-Carlo study.
Step 3: Select an allowable probability of false alarms.
Step 4: The probability of the false alarms is given by:

$$P_{FA} = \int_{-\infty}^{-th} p_0\left(x\right)dx + \int_{th}^{\infty} p_0\left(x\right)dx \tag{58}$$

where P_{FA} is the probability of false alarm, th is the selected threshold and $p_0\left(x\right)$ is the residuals probability distribution under no fault. The goal here is to select th which will yield an acceptable P_{FA}.

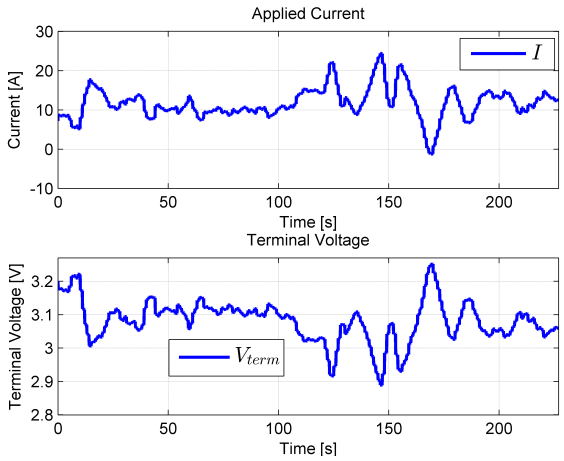

Fig. 5. Applied Current and Terminal Voltage Under No Fault Condition. Positive current corresponds with discharge.

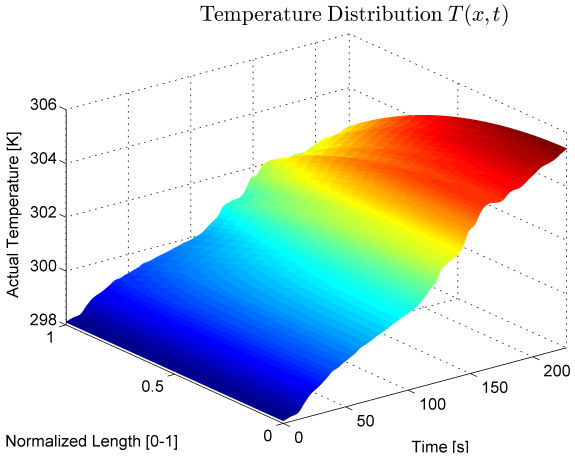

Fig. 6. Temperature distribution inside the battery Under no fault condition

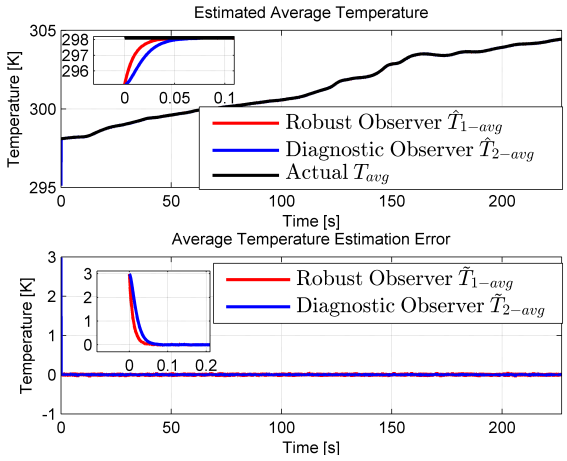

Fig. 7. Temperature estimation performance under no fault condition

IV. Simulation Studies

In this section, we conduct simulation studies to test the effectiveness of the scheme. The battery under consideration is a commercial Lithium Iron Phosphate A123 26650 cylindrical cell with rated capacity of 2.3 Ah. Battery parameters are taken from [14] and [24]. In simulation, applied current to the battery and corresponding voltage and temperature responses under no fault condition are shown in Fig. 5 and Fig. 6. To emulate a realistic scenario, we inject following zero mean Gaussian noises in the measured quantities: $10mA$ current (I) noise, 0.3^oC surface temperature (T_s) noise and $5mV$ voltage (V_{term}) noise. Under these assumed uncertainties, we select a a constant threshold value for the residual signal ($\hat{\theta}$) following the procedure discussed in the previous section. In the following results, the performance of the observers will be shown in terms of spatially averaged temperature, i.e. $T_{avg} = \int_0^1 T(x,t)dx$ and $\hat{T}_{i-avg} = \int_0^1 \hat{T}_i(x,t)dx$ where $T(x,t)$ represents actual temperature and $\hat{T}_i(x,t)$ represent estimated temperatures with $i \in \{1,2\}$. Furthermore, we will quantify the convergence performance of the estimates in terms of *convergence time* defined as the time taken to reach within $\pm 2\%$ band of the true value starting from the incorrect initial condition. The observer estimates are provided in Fig. 7 under no fault condition. To verify the convergence properties, both the observers are initialized with incorrect temperature 295 K, 3 K less than the true initial condition of 298 K. Recall from Theorem 1 that we have proven exponential stability of $\tilde{T}_1(x,t)$ to the origin, pointwise-in-space. Theorem 2 proves boundedness of the $\mathcal{L}_2$ norm of $\tilde{T}_2(x,t)$, i.e. $\|\tilde{T}_2\| \in \mathbb{L}_\infty$. In Fig. 7, both $\hat{T}_{1-avg}$ and $\hat{T}_{2-avg}$ from the *Robust Observer* and *Diagnostic Observer*, respectively, converge to the true temperature T_{avg}. The convergence time for both observers are within 0.1 sec.

Next we illustrate the effectiveness of the proposed approach under the following faulty cases.

Case 1: A constant and distributed additive heat generation fault is injected between 50 sec and 170 sec in the battery. In this case we have $\psi(T(x,t), I(t)) = 1$ and $\Delta_Q(x,t) = \theta$. The nature of the fault is abrupt/step-like. The temperature distribution is shown in Fig. 8, which clearly exhibits higher temperatures. The corresponding performance of the observers (in terms of estimated average temperature and estimation error) is provided in Fig. 9. Similar to the nominal case, both observers are initialized with incorrect temperatures to test the convergence properties. In Fig. 9, both $\hat{T}_{1-avg}$ and $\hat{T}_{2-avg}$ from the *Robust Observer* and *Diagnostic Observer*, respectively, converge to the true temperature T_{avg}. The convergence time for both observers are within 0.1 sec. This is expected, of course, since the fault does not occur until 50sec. Furthermore, the fault estimation parameter $\hat{\theta}$ crosses the threshold shortly after the fault occurrence at 50 sec, thus detecting the fault. Moreover, $\hat{\theta}$ converges to a neighborhood of the true fault size θ, as shown in the bottom subplot in Fig. 9. Recall that Theorem 2 only guarantees boundedness of $\tilde{\theta}$, i.e. $|\tilde{\theta}| \in \mathbb{L}_\infty$. Nevertheless, we find the estimate can be successfully used to estimate fault size. In this case, the detection time is 1 sec whereas the fault estimate ($\hat{\theta}$) converges to the true value (θ) within 5 sec. In addition, convergence of both observer estimates $\hat{T}_{1-avg}$, $\hat{T}_{2-avg}$ remains robust to the

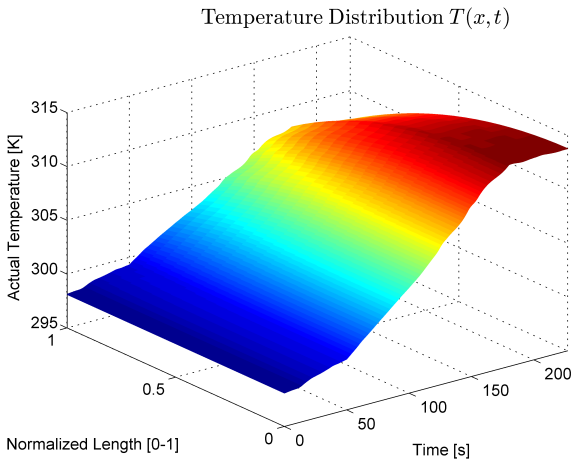

Fig. 8. Temperature distribution inside the battery under faulty condition. The fault is injected between 50 sec and 170 sec. Nature of the fault: abrupt.

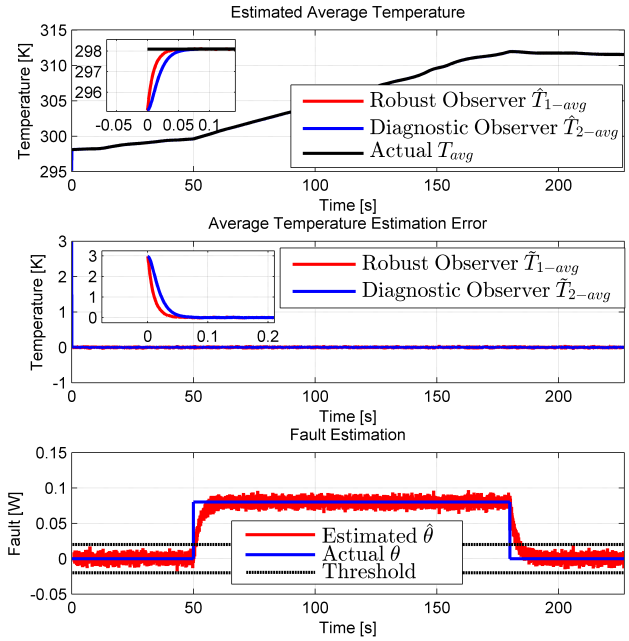

Fig. 9. Temperature and fault estimation performance under fault case 1. The fault is injected between 50 sec and 170 sec. Nature of the fault: abrupt.

fault presence.

Case 2: In this case study an internal short circuit fault has been injected at 100 sec under a constant current discharge scenario. The internal short circuit fault is characterized by internal short circuit current I_{sc} and resistance R_{sc}, and mathematically modeled by adding an additional voltage drop ($I_{sc}R_{sc}$) in the terminal voltage equation (10) and $\Delta_Q(x,t) = \theta = I_{sc}^2 R_{sc}$ in (14) [26]. Applied current, voltage, and temperature responses under the fault are shown in Fig. 10. We have chosen $I_{sc} = 25A$ and $R_{sc} = 40m\Omega$ for this case study. The nature of the fault is abrupt/step-like. The temperature distribution is shown in Fig. 11, which has faster temperature rise than the preceding two case studies. The performance of the observers (in terms of estimated

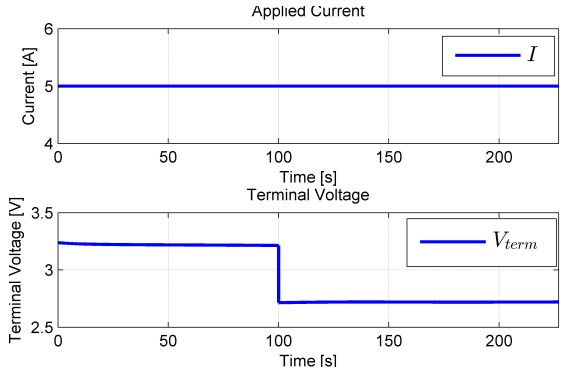

Fig. 10. Applied current and terminal voltage under the internal short circuit fault. The fault is injected at 100 sec. Nature of the fault: abrupt.

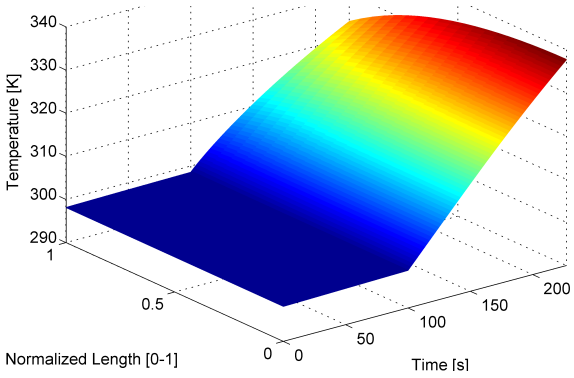

Fig. 11. Temperature distribution inside the battery under the internal short circuit fault. The fault is injected at 100 sec. Nature of the fault: abrupt.

average temperature and estimation error) is shown in Fig. 12 under the faulty condition. Similar to the nominal case, both observers are initialized with incorrect temperature to test the convergence properties. As before, both $\hat{T}_{1-avg}$ and $\hat{T}_{2-avg}$ converge to the true temperature T_{avg}. The convergence time for both observers are within 0.1 sec. Furthermore, the fault estimation parameter $\hat{\theta}$ crosses the threshold shortly after the fault occurrence at 100 sec, signaling a detected fault. Furthermore, $\hat{\theta}$ accurately estimates the fault magnitude θ, as shown in the bottom subplot in Fig. 12. The detection time is 0.2 sec and the fault estimate ($\hat{\theta}$) converges to the true value (θ) within 50 sec. Note the observers state estimates $\hat{T}_{1-avg}$, $\hat{T}_{2-avg}$ are robust to the fault presence.

V. CONCLUSIONS

This paper presents a PDE-observer based diagnostic scheme for diagnosing thermal faults in Li-ion batteries. We consider a distributed parameter thermal model coupled to a second order electrical model for diagnostic scheme design. The scheme consists of two PDE observers working in cascade. The first observer, *Robust Observer*, estimates the internal temperature distribution. We prove the distributed state estimate (i) converges exponentially to the true distributed temperature state under nominal conditions, and (ii) converges within a neighborhood of the true temperature

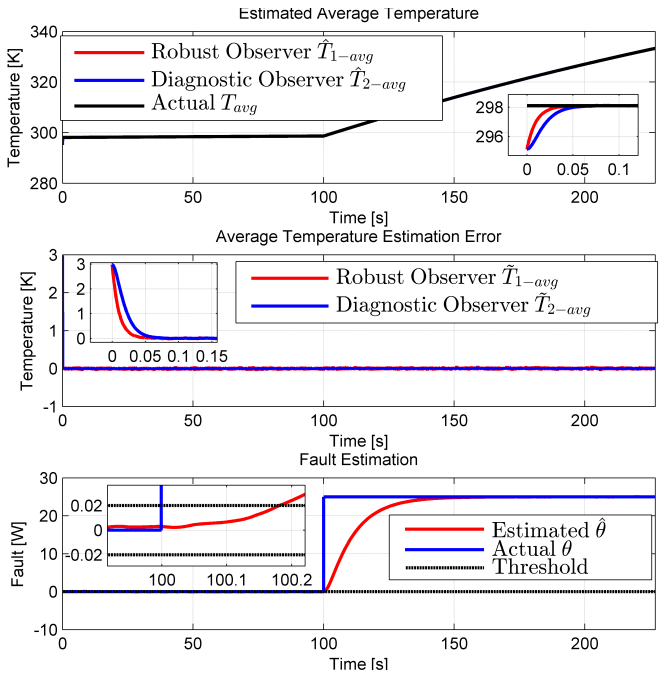

Fig. 12. Temperature and fault estimation performance under the internal short circuit fault. The fault is injected at 100 sec. Nature of the fault: abrupt.

state, which can be made arbitrarily small, under fault conditions. The second observer, *Diagnostic Observer*, utilizes this estimated temperature distribution and in turn detects and estimates thermal faults. We prove the fault estimation error $\tilde{\theta}$ is bounded in terms of the $\mathbb{L}_\infty$ norm. The proposed scheme is tested on two case studies. Case 1 considers an internal heat generation fault and Case 2 considers an internal short circuit fault. Simulation results illustrate the convergence and robustness properties of the proposed scheme. Future work includes experimental validation of the proposed scheme.

REFERENCES

[1] T. M. Bandhauer, S. Garimella, and T. F. Fuller, "A critical review of thermal issues in lithium-ion batteries," *Journal of The Electrochemical Society*, vol. 158, no. 3, pp. R1–R25, 2011.

[2] M. Charkhgard and M. Farrokhi, "State-of-charge estimation for lithium-ion batteries using neural networks and ekf," *Industrial Electronics, IEEE Transactions on*, vol. 57, pp. 4178–4187, Dec 2010.

[3] C. Gould, C. Bingham, D. Stone, and P. Bentley, "Novel battery model of an all-electric personal rapid transit vehicle to determine state-of-health through subspace parameter estimation and a kalman estimator," in *Power Electronics, Electrical Drives, Automation and Motion, 2008. SPEEDAM 2008. International Symposium on*, pp. 1217–1222, June 2008.

[4] Y. Hu and S. Yurkovich, "Battery cell state-of-charge estimation using linear parameter varying system techniques," *Journal of Power Sources*, vol. 198, pp. 338 – 350, 2012.

[5] I.-S. Kim, "The novel state of charge estimation method for lithium battery using sliding mode observer," *Journal of Power Sources*, vol. 163, no. 1, pp. 584 – 590, 2006. Special issue including selected papers presented at the Second International Conference on Polymer Batteries and Fuel Cells together with regular papers.

[6] G. L. Plett, "Extended kalman filtering for battery management systems of lipb-based {HEV} battery packs: Part 3. state and parameter estimation," *Journal of Power Sources*, vol. 134, no. 2, pp. 277 – 292, 2004.

[7] R. Klein, N. Chaturvedi, J. Christensen, J. Ahmed, R. Findeisen, and A. Kojic, "Electrochemical model based observer design for a lithium-ion battery," *Control Systems Technology, IEEE Transactions on*, vol. 21, pp. 289–301, March 2013.

[8] S. J. Moura, N. A. Chaturvedi, and M. Krstić, "Adaptive partial differential equation observer for battery state-of-charge/state-of-health estimation via an electrochemical model," *ASME Journal of Dynamic Systems, Measurement, and Control*, vol. 136, no. 1, p. 011015, 2014.

[9] S. Dey, B. Ayalew, and P. Pisu, "Nonlinear robust observers for state-of-charge estimation of lithium-ion cells based on a reduced electrochemical model," *Control Systems Technology, IEEE Transactions on*, vol. 23, pp. 1935–1942, Sept 2015.

[10] S. Dey, B. Ayalew, and P. Pisu, "Nonlinear adaptive observer for a lithium-ion battery cell based on coupled electrochemical-thermal model," *ASME Journal of Dynamic Systems, Measurement, and Control*, vol. 137, no. 11, p. 111005, 2015.

[11] X. Lin, H. Perez, J. Siegel, A. Stefanopoulou, Y. Li, R. Anderson, Y. Ding, and M. Castanier, "Online parameterization of lumped thermal dynamics in cylindrical lithium ion batteries for core temperature estimation and health monitoring," *Control Systems Technology, IEEE Transactions on*, vol. 21, pp. 1745–1755, Sept 2013.

[12] M. Debert, G. Colin, G. Bloch, and Y. Chamaillard, "An observer looks at the cell temperature in automotive battery packs," *Control Engineering Practice*, vol. 21, no. 8, pp. 1035 – 1042, 2013.

[13] R. R. Richardson, P. T. Ireland, and D. A. Howey, "Battery internal temperature estimation by combined impedance and surface temperature measurement," *Journal of Power Sources*, vol. 265, pp. 254 – 261, 2014.

[14] Y. Kim, S. Mohan, J. Siegel, A. Stefanopoulou, and Y. Ding, "The estimation of temperature distribution in cylindrical battery cells under unknown cooling conditions," *Control Systems Technology, IEEE Transactions on*, vol. 22, pp. 2277–2286, Nov 2014.

[15] J. Marcicki, S. Onori, and G. Rizzoni, "Nonlinear fault detection and isolation for a lithium-ion battery management system," in *ASME 2010 Dynamic Systems and Control Conference*, pp. 607–614, American Society of Mechanical Engineers, 2010.

[16] Z. Liu, Q. Ahmed, G. Rizzoni, and H. He, "Fault detection and isolation for lithium-ion battery system using structural analysis and sequential residual generation," in *ASME 2014 Dynamic Systems and Control Conference*, pp. V002T36A005–V002T36A005, American Society of Mechanical Engineers, 2014.

[17] S. Dey, S. Mohon, B. Ayalew, and P. Pisu, "Sensor fault detection, isolation and estimation in li-ion batteries," Submitted to IEEE Transactions on Control Systems Technology.

[18] S. Dey and B. Ayalew, "A diagnostic scheme for detection, isolation and estimation of electrochemical faults in lithium-ion cells," in *2014 ASME Dynamic Systems and Control Conference (DSCC)* (T. editor, ed.), vol. 4 of *5*, (The address of the publisher), The organization, The publisher, 7 2014. An optional note.

[19] A. Singh, A. Izadian, and S. Anwar, "Fault diagnosis of li-ion batteries using multiple-model adaptive estimation," in *Industrial Electronics Society, IECON 2013 - 39th Annual Conference of the IEEE*, pp. 3524–3529, Nov 2013.

[20] S. Mukhopadhyay and F. Zhang, "A high-gain adaptive observer for detecting li-ion battery terminal voltage collapse," *Automatica*, vol. 50, no. 3, pp. 896 – 902, 2014.

[21] S. Dey, Z. A. Biron, S. Tatipamula, N. Das, S. Mohon, B. Ayalew, and P. Pisu, "Model-based real-time thermal fault diagnosis of lithium-ion batteries," *Control Engineering Practice*, vol. 56, pp. 37 – 48, 2016.

[22] S. A. Hallaj, H. Maleki, J. Hong, and J. Selman, "Thermal modeling and design considerations of lithium-ion batteries," *Journal of Power Sources*, vol. 83, no. 12, pp. 1 – 8, 1999.

[23] M. Krstic and A. Smyshlyaev, *Boundary control of PDEs: A course on backstepping designs*, vol. 16. Siam, 2008.

[24] X. Lin, H. E. Perez, S. Mohan, J. B. Siegel, A. G. Stefanopoulou, Y. Ding, and M. P. Castanier, "A lumped-parameter electro-thermal model for cylindrical batteries," *Journal of Power Sources*, vol. 257, pp. 1 – 11, 2014.

[25] D. Doughty and E. P. Roth, "A general discussion of li ion battery safety," *Electrochemical Society Interface*, vol. 21, no. 2, pp. 37–44, 2012.

[26] W. Fang, P. Ramadass, and Z. J. Zhang, "Study of internal short in a li-ion cell-ii. numerical investigation using a 3d electrochemical-thermal model," *Journal of Power Sources*, vol. 248, pp. 1090 – 1098, 2014.